The Inverse S-Transform in Filters With Time-Frequency Localization

M. Schimmel and J. Gallart

***Abstract*—The S-transform provides a framework for data-adaptive filters which take advantage of time-frequency localized spectra. These filters basically consist in a data transformation to the time-frequency domain, the data-adaptive weighting of the localized spectra, and a back transformation. We illustrate that the inverse S-transform of manipulated spectra not necessarily transforms the localized signals as expected from the imposed weighting. The time localization is not directly translated and spurious signals and noise can be generated. We discuss this problem and suggest a new inverse S-transform, which may be helpful to many applications to take more advantage of the time-frequency localization.**

***Index Terms*—Data-adaptive filter, noise attenuation, polarization, seismic signal processing, signal detection, time-frequency analysis, time-varying filters.**

I. Introduction

The spectral content of time series generally varies due to the appearance/disappearance of different signals and noise. In seismology, for instance, the P, S, and surface waves are recorded as time varying signals with different time onsets, amplitudes, signal durations and frequency contents. Important tools to study these signals are based on time-frequency analyses. These analyses aid the signal and noise detection/identification and enable the isolation and decomposition of signals.

Many time-frequency analyses are based on windowed or short-time Fourier transforms [1]. Sliding data windows are used to obtain time-localized spectra which together put up the time-frequency representation of the data. In principle, any window function [2] can be used, but window size and shape determine the time-frequency resolution and the spectral leakage. Often Gaussian windows are used since one simultaneously achieves an optimal time and frequency resolution.

The time-frequency analyses are broadly used in image processing, medical imaging, acoustics, electrical engineering, among others. A powerful method, used in several motivating studies, is the S-transform by Stockwell *et al.* [3]. It is an extension of the short-time Fourier transform which uses frequency-dependent scaling windows in analogy to the wavelet transform. This permits a frequency-dependent resolution with narrower windows at higher frequencies and wider windows at lower frequencies. Stockwell *et al.* [3] use Gaussian windows, but other window functions can also be employed [4], [5].

The time-frequency representation obtained with the S-transform is unique and invertible. When averaged over time, the S-transform becomes the Fourier transform of the original time series. This is used to invert S-transforms and permits to transform freely between the time, frequency and time-frequency domain. All these signal representations are equally valid, but the signal components may separate better in one domain. The simultaneous localization in time and frequency often permits signal isolation and filters can be constructed to operate on the S-spectra before their back transformation to time. These filters consist of the data adaptive weighting of the spectral components due to a measure which separates to some extend signals from noise (e.g., degree of polarization, coherence, or energy). The higher weights localize regions in the time-frequency spectrum which are expected to be the signal components while the lower weights attenuate undesired noise. The inverse S-transform is computed to reconstruct the filtered time series from the weighted S-spectrum.

This filter procedure has been employed by Pinnegar and Eaton [6] to filter seismic record sections by their averaged S-spectra. Zhu *et al.* [7] and Goodyear *et al.* [8] use S-spectra to remove motion-related artifacts caused by respiratory/cardiac activity, blood flow and other fluctuations from medical magnetic resonance images. The image pixel time courses of these analyses are transformed to the time-frequency domain where the identified artifacts are down-weighted before the back transformation to the time domain.

This communication focuses on the realization of the back or inverse transform in filters which operate on the S-spectra. We show that the back-transformation of manipulated S-spectra does not transform the localized signals as expected from their manipulation. The back transformed data can have increased noise levels and embedded spurious signals. These features can appear at all possible times and are therefore not easily detected. We point to this concern and suggest a new approach which bypasses the time averaging of localized spectra during the inverse transform.

II. Time-Frequency Localization With S-Transform

A. Localized Spectra Determination With Generalized S-Transform

The S-transform of a time series $u(t)$ is following Stockwell *et al.* [3]

$$S(\tau, f) = \int_{-\infty}^{\infty} u(t) w(\tau - t, f) e^{-i2\pi f t} dt \tag{1}$$

with Gaussian window

$$w(\tau - t, f) = \frac{|f|}{k\sqrt{2\pi}} e^{\frac{-f^2(\tau - t)^2}{2k^2}}, \quad k > 0. \tag{2}$$

f is the frequency and τ and t are time variables. τ is the center time of the Gaussian window and k is a scaling factor which controls the number of oscillations in the window. k permits to control the time-frequency resolution. That is, the frequency resolution increases with k on costs of the time resolution whenever the increased windows sample more of the investigated signal. A high precision in both, time and frequency, can not be obtained due to the uncertainty principle. An increased frequency resolution can be useful for the separation of time interfering signals. Stockwell *et al.* [3] write (1) and (2) as a product of spectra (3) which facilitates the implementation on a computer

$$S(\tau, f) = \int_{-\infty}^{\infty} U(\alpha + f) e^{-\frac{2\pi^2 k^2}{f^2}\alpha^2} e^{i2\pi\alpha\tau} d\alpha, \quad f \neq 0. \tag{3}$$

$U(\alpha)$ is the Fourier transform of $u(t)$ and is calculated only once. $U(\alpha)$ is shifted by f before it is multiplied with the window function. $S(\tau, f)$ is then achieved applying the inverse Fourier transform.

B. Inverse Transformation of S-Spectra

1) Routinely Used Approach: The local time-frequency spectra $S(\tau, f)$ obtained with the generalized S-transform can easily be

Manuscript received June 22, 2004; revised January 11, 2005. This work was supported by the Spanish Ministry of Education and Science through the Ramon and Cajal Program. The associate editor coordinating the review of this paper and approving it for publication was Prof. Zixiang Xiong.

The authors are with the Institute of Earth Sciences Jaume Almera-CSIC, c/Lluis Sole i Sabaris, s/n, 08028 Barcelona, Spain (e-mail: schimmel@ija.csic.es).

Digital Object Identifier 10.1109/TSP.2005.857065

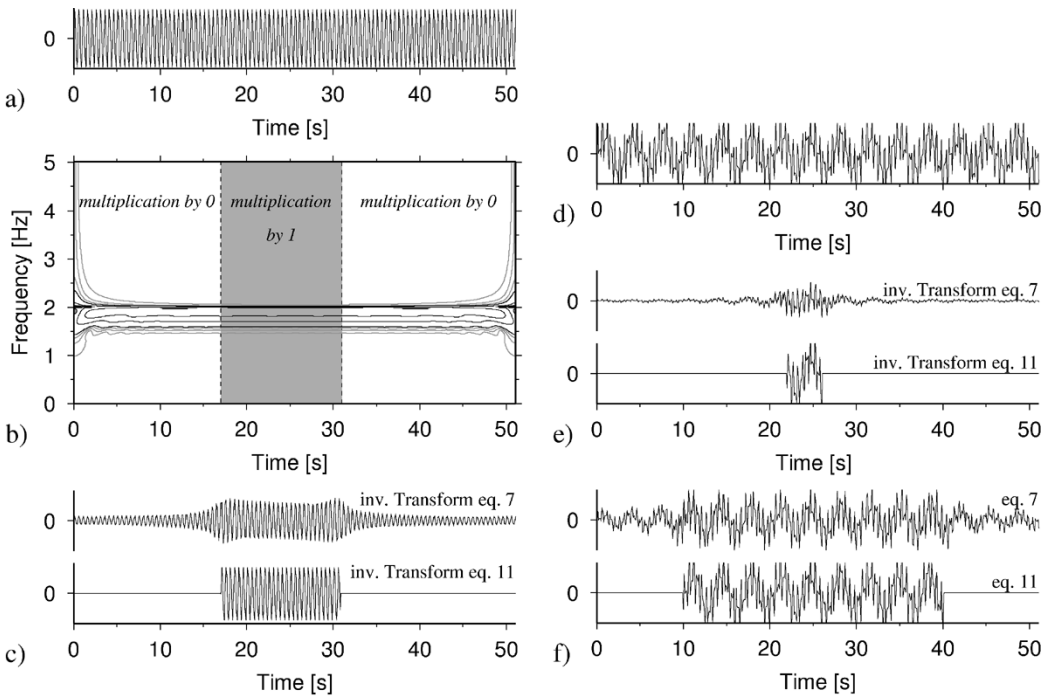

Fig. 1. (a) Two-hertz sine wave and (b) its amplitude S-spectrum. The black lines have a contour interval of 20% of the maximum amplitude and the grey lines contour the lower 20% with a 5% increment. The shaded background indicates the S-spectrum manipulation. (c) Results of the back transformation of the manipulated S-spectrum. (d) A second test trace constructed from three sine functions with 0.3-, 2-, and 3.5-Hz frequencies. The corresponding S-spectrum has been manipulated similar to (b), however, with a 5-s and 30-s time duration of the band-pass. The back transformed time series are shown in (e) and (f), respectively.

back-transformed (e.g., [3] and [5]) since the S-transform windows satisfy the condition

$$\int_{-\infty}^{\infty} w(\tau - t, f)d\tau = 1. \tag{4}$$

This ensures that the time averaging of the S-spectrum $S(\tau, f)$ yields the spectrum $U(f) = FT[u(t)]$, as shown in (5)

$$\int_{-\infty}^{\infty} S(\tau, f)d\tau = \int_{-\infty}^{\infty} u(t)e^{-i2\pi ft} \int_{-\infty}^{\infty} w(\tau - t, f)d\tau dt = U(f) \tag{5}$$

It means that the S-transform is exactly invertible with one inverse Fourier transform. This permits a fast and easy retrieval of the time series from their S-spectrum. If the spectrum is manipulated then the back transformation provides the filtered time series. A manipulation of the spectrum can be the weighting of the different spectral components based on criteria such as coherence, polarization, energy, etc. to enhance/attenuate certain features in the data. This procedure permits to eliminate undesired parts of the data in the time-frequency domain. Equations (6) and (7) express this filter strategy with $F(\tau, f)$ as a data-adaptive time-frequency weight function.

$$U_{filt_1}(f) = \int_{-\infty}^{\infty} S(\tau, f)F(\tau, f)d\tau \tag{6}$$

$$u_{filt_1}(t) = \int_{-\infty}^{\infty}\int_{-\infty}^{\infty} S(\tau, f)F(\tau, f)e^{+i2\pi ft}d\tau df \tag{7}$$

where $F(\tau, f)$ is real, and any complex function would manipulate the phase spectrum.

2) New Approach: A second concept can be derived.With the Gaussian window $(k\sqrt{2\pi}/|f|)w(\tau - t, f)$ we obtain the time-time representation of the windowed time series $u(t)$

$$x(\tau, t) = u(t)e^{\frac{-f^2(\tau-t)^2}{2k^2}} \tag{8}$$

which for any frequency f (and $k > 0$) reduces to $u(t) = x(t, t)$ at $\tau = t$. After the Fourier transform of (8), one recognizes the relation with the S-spectrum (1) and (2).

$$x(\tau, f) = \frac{k\sqrt{2\pi}}{|f|}S(\tau, f) \tag{9}$$

And therefore, the original time series $u(t)$ can be retrieved from the weighted S-spectrum through the "diagonal elements" of the time-time representation obtained with following back transformation:

$$u(t) = k\sqrt{2\pi}\int_{-\infty}^{\infty} \frac{S(t, f)}{|f|}e^{+i2\pi ft}df. \tag{10}$$

The filtered trace, in analogy to $u_{filt_1}(t)$, is expressed as

$$u_{filt_2}(t) = k\sqrt{2\pi}\int_{-\infty}^{\infty} \frac{S(t, f)F(t, f)}{|f|}e^{+i2\pi ft}df. \tag{11}$$

In contrast to (7) the phasor is assigned with the time variable of the S-spectrum and its weight, and therefore conserves the time localization imposed by the weight. This time localization has been lost in the summation over τ (6) and the inverse Fourier transform. The factor $k\sqrt{2\pi}/|f|$ cancels with the frequency dependent amplitude of the Gauss window $w(\tau - t, f)$ used to determine $S(t, f)$.

C. Differences for Manipulated S-Spectra

The differences between both strategies (7) and (11) can be shown with a hypothetical filter $F(t = t_1, f) = 1$ and $F(t \neq t_1, f) = 0$ else-

where. That is, at time $t = t_1$ all frequency components of the S-spectrum are passed while at all other times and frequencies the S-spectrum is suppressed by $F(t, f)$. Employing this operation, (6) reduces to $U_{filt_1}(f) = S(t_1, f)$, which becomes

$$u_{filt_1}(t) = \int_{-\infty}^{\infty} S(t_1, f) e^{+i2\pi ft} df \tag{12}$$

in the time domain. Each frequency component $S(t_1, f)$ is transformed to a sine wave which together may cancel or not at $t \neq t_1$. One observes that the zero weight of $F(t, f)$ at $t \neq t_1$ does not directly map into the time domain. With the second approach (11), one obtains

$$u_{filt_2}(t_1) = \int_{-\infty}^{\infty} \frac{k\sqrt{2\pi}}{|f|} S(t_1, f) e^{+i2\pi f t_1} df$$

$$\text{and} \quad u_{filt_2}(t \neq t_1) = 0 \tag{13}$$

which shows that the time localization through the $F(t, f)$ translates directly into the time domain.

Fig. 1 illustrates this in an extended example. The test trace $u(t)$ is a 2-Hz sine wave, as depicted in Fig. 1(a). The time frequency representation in Fig. 1(b) shows the amplitudes of the S-spectrum. (Note that $k = 1$ is used throughout all examples.) In the next step the S-spectrum is manipulated by multiplying all spectral components in the white area [Fig. 1(b)] by zero. The manipulated spectrum is then back transformed to the time domain using both concepts [Fig. 1(c)]. It is visible from the filtered traces that only with the second strategy the imposed time localization translates directly to the time domain in analogy to (13)

For a further test we add three sine functions of 0.3-, 2-, and 3.5-Hz frequencies [Fig. 1(d)]. Its S-spectrum has been manipulated similarly to previous example. However, we use a time duration of 5 s and 30 s for the pass-band (multiplication by 1) and show the filtered signals in Figs. 1(e) and 1(f), respectively. The examples demonstrate that there are no zero amplitude stretches as one would expect from the imposed S-spectrum manipulation, when applying the first inversion strategy. Instead, one observes due to linearity the superposition of sine waves, each generated as in (12). The zero amplitude weights are not sufficient to guarantee a cancellation of the sine waves in the time domain.

Note that the S-transform of none of the filtered traces would reproduce the manipulated S-spectrum. The S-spectrum of the filter output of the first approach has energy at the frequencies of the sine functions at all times. The S-spectrum of the filtered trace with the second approach has smeared amplitudes at the begin and end of the nonzero amplitude signal. We therefore understand the back transform of the manipulated spectrum as part of the filter operation.

For Fig. 2, a time (and frequency) limited chirp function is used. Its amplitude S-spectrum is shown in Fig. 2(b). The black lines contour the amplitude S-spectrum with a 20% amplitude increment. The lower-most 20% amplitudes are shown with the grey lines and a 5% contour interval. The dashed lines in Fig. 2(b) define regions labeled by W1, W2, W3 and W4. In this example we wish to suppress the chirp signal and multiply the S-spectrum within the regions defined by W1, W2, W3, and W4 with zero. Figs. 2(c)–(f) show the filtered traces using (7) and Fig. 2(g) shows the results with (11), respectively. The results obtained with the latter approach are the same for the 4 windows and have been plotted on top of each other. The manipulated S-spectrum has not been smoothed and the rough edges at about 19 and 28 s map into the time domain. The application of a taper in the time-frequency domain removes these signatures. Striking are the different responses of the S-spectrum manipulation in Figs. 2(c)–(f). The longer the windows W1, W2, ... the better is the desired suppression of the chirp signal. The reason for this is that the S-spectrum [Fig. 2(b)] contains very small amplitudes at $t < 19$ s and $t > 28$ s. These signals are caused by the chirp function and due to the finite width windows $w(\tau - t, f)$ of the S-transform. This energy from outside the windows W1, W2, and W3 is not suppressed and maps with the first approach, corresponding its phase spectrum, to a small signal between 19 and 28 seconds. That is, it maps to its origin. This is not the case for the second approach since one inverts each local spectrum as function of time directly to the window center time.

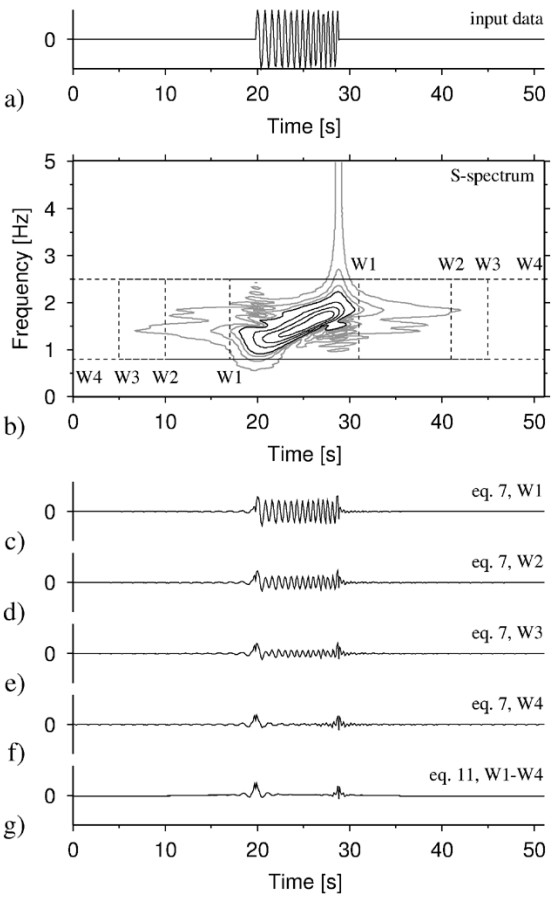

Fig. 2. (a) Time series is a time limited chirp function. (b) Amplitude S-spectrum of the data from a). The contour intervals are 5% (grey lines) and 20% (black lines) of the maximum amplitude. Grey lines are used until 20%. W1–W4 label four different regions in which the spectrum is multiplied by zero. The traces in (c)–(f) show the back transformed signals using (7). In (g), we show the results applying (11). The four traces are plotted on top of each other. Note that in no case was a taper applied to smooth the edges in the manipulated S-spectrum.

D. Examples With Data-Adaptive Polarization Filter

Previous case studies demonstrate that the filter efficiency depends on the inverse transform. Data and manipulation have been constructed to point to these differences. Now we consider an authentic data-adaptive filter which we apply to a theoretical and real data set to illustrate differences and importance for a realistic situation.

We use three-component (3-c) data and apply a polarization filter to enhance arbitrarily polarized signals in the data. In essence, the filter consists in the determination of a frequency dependent degree of polarization (dop) which we use to weight the S-spectra. The dop is taken from Schimmel and Gallart [9]. It is an instantaneous measure on how well a signal is polarized based on the stability of its arbitrary polarization within a small sliding data window. It assigns at each time and frequency a real number between 0 and 1 which is used to weight the components of the S-spectrum in analogy to $F(t, f)$ in (7) and (11).

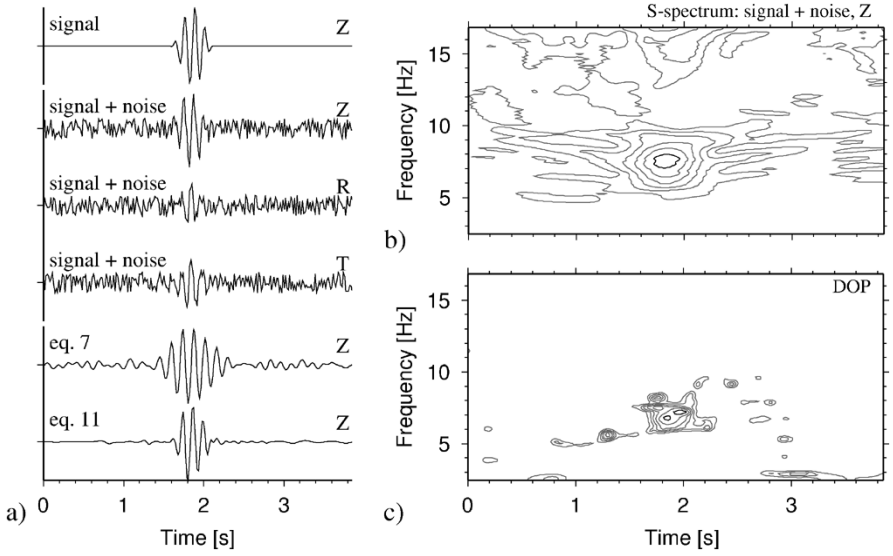

Fig. 3. (a) From top to bottom: The noise-free signal on a vertical component (Z) registration, the noise contaminated Z, radial (R), and transverse (T) components, and the polarization filtered Z components employing (7) and (11). (b)–(c) The contour plots display the amplitude S-spectrum (Z component) and the degree of polarization (dop) for the noisy data. dop measures the instantaneous polarization and ranges between 0 and 1, with 1 indicating perfect signal polarization.

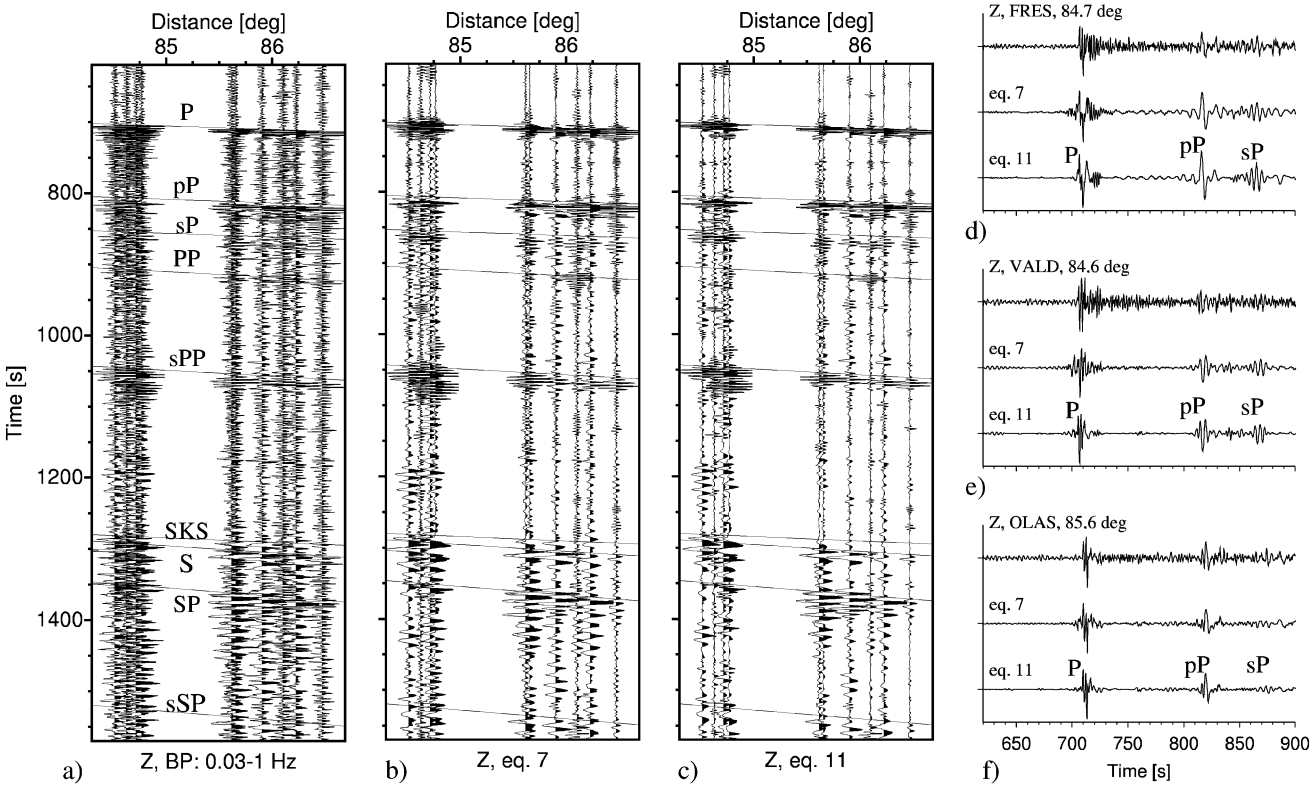

Fig. 4. (a) Z component seismograms for an earthquake at Primor in Russia (2003 July 27) recorded at ten mobile stations in NW Spain. Data are band-passed (0.03–1 Hz) and the labels indicate some main seismic signals. (b) Polarization filtered record section. The approach, (7), is used for the inverse transform to the time domain. (c) Same as (b) but employing (11). (d)–(f) display a data zoom to enable inspection of the wave forms at three selected stations.

Components with a low dop are down weighted to enhance/isolate the polarized signal with a high dop.

The example in Fig. 3 uses a theoretical 3-c registration of a polarized signal. In Fig. 3(a) we show from top to bottom: The noise free signal on the vertical component (Z), the noise contaminated vertical (Z), radial (R), and transverse (T) components, and the polarization filtered Z components obtained with both approaches. White noise is used to contaminate the polarized signal.

Both, the amplitude S-spectrum of the noisy Z component and the dop are contoured in Figs. 3(b) and 3(c), respectively. It can be observed that the dop is largest for the polarized signal. Some smaller features are visible in Fig. 3(c), but belong to the background noise which occasionally can be polarized. The dop functions as mask and isolates signals from noise. The two lower-most traces in Fig. 3(a) are the Z component filter outputs. The overall noise has been attenuated with both approaches, however, the filter output obtained with (11) mostly

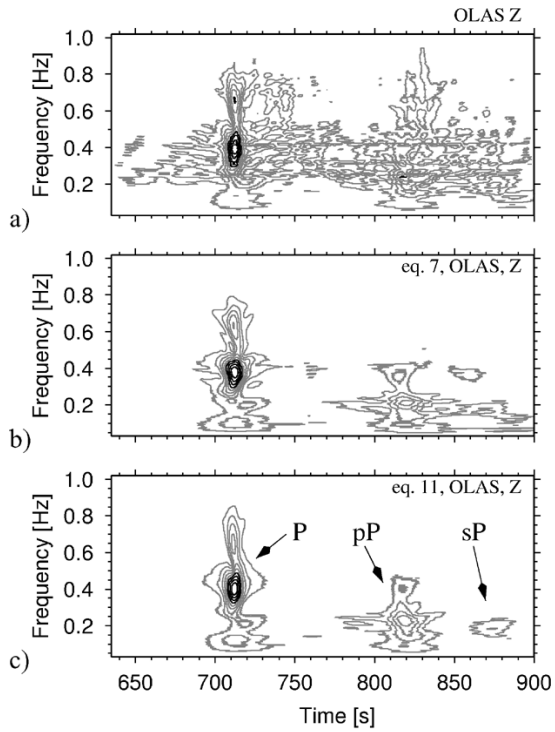

Fig. 5. (a) Amplitude S-spectrum of the Z record of station OLAS [first trace in Fig. 4(f)]. The amplitudes are normalized to 1 and the contour interval is 0.2. The black lines indicate amplitudes larger than 0.6. (b) Same as (a) but for the filter output obtained with inverse transform (7) [second trace in Fig. 4(f)]. (c) Same as (b) but using (11) [third trace in Fig. 4(f)].

resembles to the noise-free test signal. The potential of this filter is best exploited employing the second approach as inverse transform.

In the following example, we use 3-c seismic recordings of an earthquake with epicenter at Primor in Russia (2003 July 27, $47^{\circ}\mathrm{N}$, $139^{\circ}\mathrm{E}$, 470 km depth, $m_b = 6.3$) recorded at 10 mobile broad-band stations in NW Spain. Fig. 4(a) shows the corresponding Z components after band passing (0.03–1 Hz). The labels and lines indicate the expected arrivals of some prominent seismic phases. The first seismic wave from the Earthquake arrives as the P phase at about 700 s. The other phases are reverberations or wave type conversions at the Earth surface. The P-wave and S-wave coda consists of many other reverberations and wave-type conversions at the different structural discontinuities in the Earth. The signals before 700 s provide an estimate of the background noise in the data. Several seismic arrivals are already visible in the band-passed data [Fig. 4(a)].

We apply the polarization filter from the previous example to enhance the polarized signals. The data adaptive filter is used in its simplest form on the individual traces without any lateral averaging of the dop or the waveforms to aid the attenuation of incoherent noise. The lateral averaging would further enhance coherent polarized signals through the attenuation of isolated polarized features which likely are polarized noise.

Fig. 4(b) and 4(c) shows the filtered Z components. An overall noise suppression is visible and several signals have been enhanced. Further, it seems that the polarized signals lack the higher frequency components at increasing time. This is mainly attributed to attenuation due to scattering and inelasticity and the increased appearance of shear waves (S-waves) at larger time. Isolated polarized signals are attributed to polarized noise which can be due to some other local event/happening which is recorded. Seismic waves scattered at local heterogeneities can also be polarized and are often classified as signal generated noise.

The differences between Fig. 4(b) and (c) are caused by the different approaches to transform the manipulated S-spectra to time. Figs. 4(d)–(f) are zooms of the filter input and outputs for three of the stations. It is visible that the noise level is smaller with (11) than with (7). Part of the signals in Fig. 4(b) [second traces in Figs. 4(d)–(f)] is introduced by the transform. Both approaches have been tested with data from several earthquakes and different filter settings. It is observed that differences between both transformations can be larger than shown in Fig. 4. The dop is a complicated function and how much signals are introduced by the transform depend on the duration of the polarized signal and the contrast to the dop values of the signal surrounding.

The amplitude S-spectra of the traces for station OLAS [Fig. 4(d)] are displayed in Fig. 5(a)–(c). The first arrival P and the event-site surface reflections pP and sP are visible in the three amplitude spectra. Fig. 5(b) and (c) are cleaned images of the input data due to the applied polarization filter. In Fig. 5(c), the signals appear more distinguished. This observation can be more or less pronounced for other data. The problem with real data is that it is not exactly known what is signal (and what is noise). This complication can obscure the filter performance and synthetic simulations become important for the interpretation.

III. Discussion and Conclusion

This paper proposes a new strategy for the inverse S-transform. This is shown to be relevant when the data processing involves a manipulation of the S-spectrum for feature extraction or noise attenuation. Our approach works differently to the routine inverse S-transform by Stockwell *et al.* [3]. Inherent to the differences, both approaches provide different results whenever the spectrum is altered.

With the approach by Stockwell *et al.* [3] the S-spectrum is averaged over time to obtain the Fourier spectrum of the input data. This provides a computational efficient and simple way to freely move between the equally valid signal representations in the time, the frequency, and the time-frequency domain. However, we show that weighting the amplitude S-spectrum to isolate/enhance signals can lead due to the newly weighted Fourier spectrum to a reconstructed time series with energy appearing at undesired places. It is shown in our examples that the imposed time localization through the weighting does not directly translate to the time domain. As a consequence, one does not really take advantage of the signal localization and isolation in the S-spectrum.

Our approach avoids the time averaging and is based on the individual consideration of each local spectrum as function of time (window center time). Each of these spectra is back transformed directly to the time that equals the window center time. This alternative strategy by-passes the need to average the local spectra and the signal localization in time translates directly to the filtered time series.

In fact, we consider the back transform as part of the filter since it may depend on the manipulation, its purpose, and the data at hand which strategy one should prefer. For our purposes, the alternative back transform increases the quality of the filter outputs. There are less noise and less spurious signals, and the waveforms seem to be less distorted. In any case, the results must be interpreted with care and with respect to the applied settings. Further, a complete reconstruction of the waveforms should not be expected in the presence of large noise since corrupted signal components will also be down-weighted.

It would seem from the examples given here that our approach can be useful to other applications based on the different weight functions. In our examples, we employ the degree of polarization to isolate polarized signals. The degree of polarization reduces to a real number weighting such as other functionals based on other physical principals. Therefore, one could expect that our alternative inverse transform is helpful to similar methods, such as the prestack noise attenuation filter

by Pinnegar and Eaton [6], the removal of motion related artifacts in medical magnetic resonance images ([7], [8]) and other methods which apply a similar recipe. Whether the differences are large and justify a change of strategy dependents on the data and weight.

Concerning the dop we like to add that the polarization is subject to noise and that noise corrupted signals (noise interference in time and frequency) might not be detected by the approach. Further, noise can be polarized, for instance if noise amplitudes are larger on one component than on the others and may not be suppressed. For densely spaced data such as a seismic record section, the isolated noise can be attenuated by lateral averaging of the dop ([9], [10]). This improves considerably the signal detection through polarization. Noise suppression through averaging the degree of polarization is an alternative to average waveforms or covariance matrices. It has the advantage that one does not attenuate polarized signals with laterally changing waveforms which may happen in the transmission to post-critical reflections or due to focusing by heterogeneities.

REFERENCES

[1] D. Gabor, "Theory of communication," *J. Inst. Elect. Eng.*, vol. 93, no. 26, pp. 429–457, 1946.

[2] F. J. Harris, "On the use of windows for harmonic analysis with the discrete Fourier Transform," *Proc. IEEE*, vol. 66, no. 1, pp. 51–83, Jan. 1978.

[3] R. G. Stockwell, L. Mansinha, and R. P. Lowe, "Localization of the complex spectrum: the S transform," *IEEE Trans. Signal Process.*, vol. 44, no. 4, pp. 998–1001, Apr. 1996.

[4] P. D. McFadden, J. G. Cook, and L. M. Forster, "Decomposition of gear vibration signals by the generalized S transform," *Mechan. Syst. Signal Process.*, vol. 13, pp. 691–707, 1999.

[5] C. R. Pinnegar and L. Mansinha, "The S-transform with windows of arbitrary and varying shape," *Geophysics*, vol. 68, pp. 381–385, 2003.

[6] C. R. Pinnegar and D. E. Eaton, "Application of the S transform to prestack noise attenuation filtering," *J. Geophys. Res.*, vol. 108, no. B9, p. 2422, 2003.

[7] H. Zhu, B. G. Goodyear, M. L. Lauzon, R. A. Brown, G. S. Mayer, A. G. Law, L. Mansinha, and J. R. Mitchell, "A new local multi-scale Fourier analysis for medical imaging," *Med. Phys.*, vol. 30, pp. 1134–1141, 2003.

[8] B. G. Goodyear, H. Zhu, R. A. Brown, and R. Mitchell, "Removal of phase artifacts from fMRI data using a Stockwell Transform filter improves brain activity detection," *Magn. Resonance Med.*, vol. 51, pp. 16–21.

[9] M. Schimmel and J. Gallart, "Degree of polarization filter for frequency dependent signal enhancement through noise suppression," *Bull. Seism. Soc. Amer.*, vol. 94, pp. 1016–1035, 2004.

[10] M. Schimmel and J. Gallart, "The use of instantaneous polarization attributes for signal detection and image enhancement," *Geophys. J. Int.*, vol. 155, pp. 653–668, 2003.

[11] P. Wessel and W: H. F. Smith, "Free software helps map and display data," *EOS Trans. Amer. Geophys. Un.*, vol. 72, no. 441, pp. 445–446, 1991.